

Field enhancement and molecular response in surface-enhanced Raman scattering and fluorescence spectroscopy

Mikael Käll,^{1*} Hongxing Xu² and Peter Johansson³

¹ Department of Applied Physics, Chalmers University of Technology, S-412 96 Göteborg, Sweden

² Division of Solid State Physics, Lund University, Box 118, S-221 00 Lund, Sweden and Institute of Physics, Chinese Academy of Science, Beijing 100080, China

³ Department of Natural Sciences, University of Örebro, S-701 82 Örebro, Sweden

Received 20 November 2004; Accepted 17 February 2005

We present a theoretical analysis of surface-enhanced Raman scattering and fluorescence emission from chromophoric molecules located at electromagnetic 'hot spots' in nanoparticle aggregates. The model combines classical electrodynamic enhancement effects with molecular quantum dynamics and allows us to quantify various molecular cross-sections and spectral properties. For a model molecule that simulates rhodamine 6G, we find that an electromagnetic Raman enhancement of the order of 10^{10} results in an effective Raman cross-section of the order of 10^{-14} cm², in agreement with single-molecule Raman measurements. Copyright © 2005 John Wiley & Sons, Ltd.

KEYWORDS: field enhancement; molecular quantum dynamics; plasmons; surface-enhanced Raman scattering; fluorescence

INTRODUCTION

Soon after the discovery of surface-enhanced Raman scattering (SERS),¹ Moskovits² put forward an interpretation of the phenomenon in terms of electromagnetic resonances in noble metal nanostructures. This paved the way for the 'electromagnetic SERS theory', which has since been the subject of numerous studies and is now generally accepted, in several variants, as the fundamental basis for the surface-enhancement effect. The electromagnetic resonances of interest, now often called localized surface plasmons (LSPs), involve collective conduction electron excitations in isolated or electromagnetically coupled metal nanostructures, which can be particles, rods, cavities, surface protrusions, etc. The resonances are closely related to surface plasmon polaritons (SPPs) at flat surfaces,³ e.g. LSPs can often be interpreted in terms of coupled standing SPP waves. Hence SERS is an integral part of the emerging field of 'plasmonics' (for a recent review of some aspects, see Ref. 4), which involves applications and phenomena as diverse as enhanced transmission⁵ and fluorescence resonance energy transfer⁶ in thin metal films, surface plasmon resonance biosensing,⁷ photodynamic therapy using plasmonic nanoshells⁸ and optical transmission lines based on nanoparticles.⁹

In 1997, Nie and Emory¹⁰ and, independently, Kneipp *et al.*¹¹ reported on the observation of single molecules using SERS. The enhancement factors estimated from these measurements, of the order of 10^{15} , were much higher than previously known, which once again raised questions regarding the fundamental mechanism(s) behind SERS. In this paper, we outline a theory of SERS from resonant molecules located in the gap between metal nanoparticles, a configuration which we argue provides the most reasonable interpretation of single-molecule SERS. The model unites aspects of both the electromagnetic enhancement and the molecular dynamics, and includes both Raman and fluorescence processes. A detailed account of the model can be found in Refs. 12 and 13. The main message is that the calculated *absolute* Raman cross-section is in good agreement with experiment and, therefore, that no additional processes beyond the established electromagnetic enhancement mechanism need to be invoked in order to explain single-molecule SERS from resonant molecules.

FIELD ENHANCEMENT

The electromagnetic field that accompanies the resonant electron motion in a plasmonic system is in general of near-field (evanescent) character and, because of the spatial confinement, enhanced compared with the excitation field by a factor $M(\omega)$. Although it is extremely difficult to

*Correspondence to: Mikael Käll, Department of Applied Physics, Chalmers University of Technology, S-412 96 Göteborg, Sweden.
E-mail: kall@fy.chalmers.se

directly measure this factor, various types of electrodynamic calculations regularly produce values up to 10^3 . However, the magnitude of the field enhancement factor at a given optical frequency ω , at a given point in space and at a particular illumination configuration depends crucially on the composition, size, shape and arrangement of the metal nanostructure, and such high values are only expected under special circumstances. In particular, ultra-high field enhancement factors generally require the concerted action of an electrostatic contribution, such as the ‘lightning rod effect’,¹⁴ and an LSP resonance excitation. This is also the case for gaps in nanoparticle aggregates, on which we focus below. A molecule situated in such a ‘hot spot’ thus experiences an excitation intensity that is enhanced by a factor $|M(\omega)|^2$ compared with the incident intensity. Also, the far field radiated by the molecule is enhanced by the factor $M(\omega)$, where ω now denotes the emission frequency, which means that the overall Raman enhancement factor is proportional to $|M|^4$. Moreover, the spontaneous emission rate and the damping of molecular excitations, because of losses to the metal particles, for example by creation of electron–hole pairs, are enhanced, in this case by a factor $|M_d(\omega)|^2$. The factors $M(\omega)$ and $M_d(\omega)$ are similar in magnitude unless the molecule–particle separation is small (a few nanometers or less), in which case $M_d(\omega)$ becomes considerably larger than $M(\omega)$.

In Fig. 1, we show an electrodynamic calculation of the spatial distribution of the intensity enhancement, based on extended Mie theory,^{15,16} for an aggregate composed of

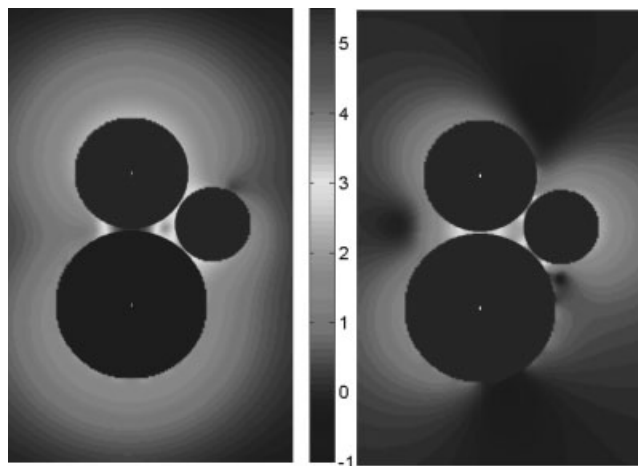


Figure 1. Spatial distribution of the intensity enhancement factor $|M(\omega)|^2$, displayed on a logarithmic scale, in a plane through the centers of three dissimilar Ag spheres ($R_1 = 40$ nm, $R_2 = 30$ nm, $R_3 = 20$ nm) in air at an illumination wavelength of $\lambda = 508$ nm, corresponding to a photon energy of $\hbar\omega = 2.44$ eV, for vertical polarization to the left and horizontal polarization to the right. The surface-to-surface distances are $2d = 10$ Å for all three gaps and the incident wavevector is perpendicular to the plane of the figure.

three silver nanospheres of different radii. The calculation illustrates the existence of several ‘hot spots’ at various locations within the nanosphere aggregate, and also the presence of ‘cold’ regions, where the field is excluded and the enhancement is below unity. The main ‘hot spot’ is located in the gap between the two largest Ag spheres, where the intensity enhancement reaches a value of $\sim 5 \times 10^5$ for the transverse polarization configuration. However, if the incident polarization is turned 90° , the enhancement drops by several orders of magnitude at this site, but in turn increases at the two other gap positions. This dramatic polarization dependence is largely in accord with recent experiments on isolated nanoparticle aggregates.^{17,18}

In Fig. 2, we show the intensity enhancement spectrum $|M(\omega)|^2$ for the midpoints in the three gaps in the aggregate. The pronounced peaks in the energy dependence are due to various ‘hybridized’ LSP excitations, built up through combinations of the fundamental single-sphere multipolar resonances. It should be noted that the calculation takes into account multipoles up to order 20, and that a model based only on dipoles is an extremely poor representation of the full calculation. The main reason for this is that the enhancement in the gap regions includes a dominant electrostatic contribution.¹⁹ For a dimer system composed

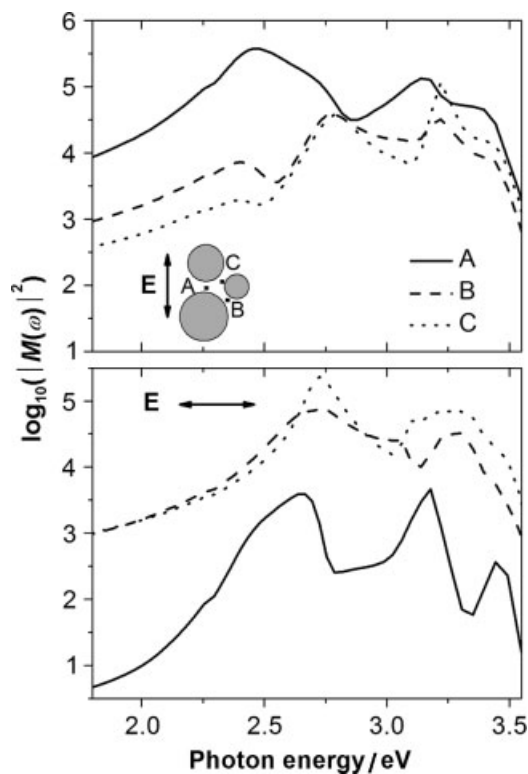


Figure 2. Intensity enhancement spectra $|M(\omega)|^2$ at the midpoints of the three gaps A (solid line), B (dashed line) and C (dotted line), as indicated in the inset, for the three-sphere system shown in Fig. 1. The calculations include multipoles up to order $L = 20$, which is close to convergence.

of two spheres with radii R_i and R_j , and for an incident polarization parallel to the dimer axis, the electrostatic intensity enhancement scales as $M = 1 + (R_i + R_j)/2d$, where $2d$ is the gap size.

INCLUDING MOLECULAR DYNAMICS

The most important ingredients of our molecular model are illustrated in Fig. 3. The molecule, which is placed at the midpoint between two Ag spheres, has two electronic levels differing in energy by $\hbar\Omega_{ge}$ and a vibrational mode with energy quantum $\hbar\Omega_{vib}$ and damping rate γ_{vib} , which determine the wavenumber and linewidth, respectively. We include a number of vibrational levels per electronic level in the model. The electron–vibration coupling that makes Raman scattering possible is included via a Franck–Condon mechanism; the equilibrium position of the vibrational mode is displaced a distance x_0 upon electronic excitation. The strength of the electron–vibration coupling is described by the dimensionless parameter

$$\alpha = \frac{x_0}{\sqrt{\frac{2\hbar}{\mu\Omega_{vib}}}} \quad (1)$$

where μ is the reduced mass associated with the vibrational degree of freedom. The absorption spectrum and the Raman scattering profile for the model molecule in free space (hence without enhancement effects), calculated using lowest order perturbation theory, are shown in Fig. 4. We chose parameter values to obtain an absorption spectrum similar to that of rhodamine 6G (R6G), a highly fluorescent molecule that is often studied in single-molecule SERS experiments. The experimental absorption spectrum for R6G is also shown

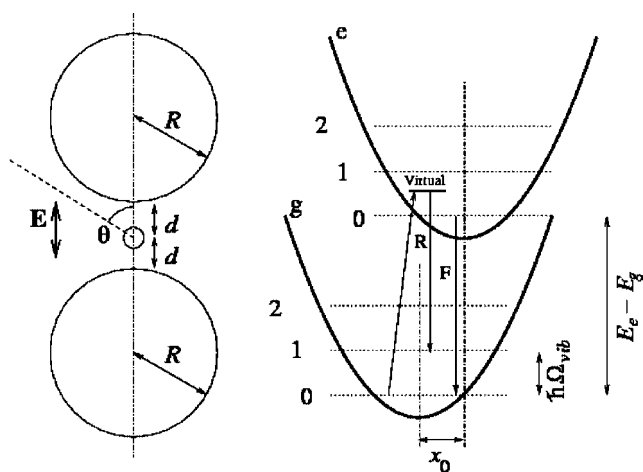


Figure 3. Schematic illustration of the molecule model and the processes leading to fluorescence (marked F, involving a real transition from the upper to the lower electronic state) and Raman scattering (marked R), which involves an intermediate, virtual state.

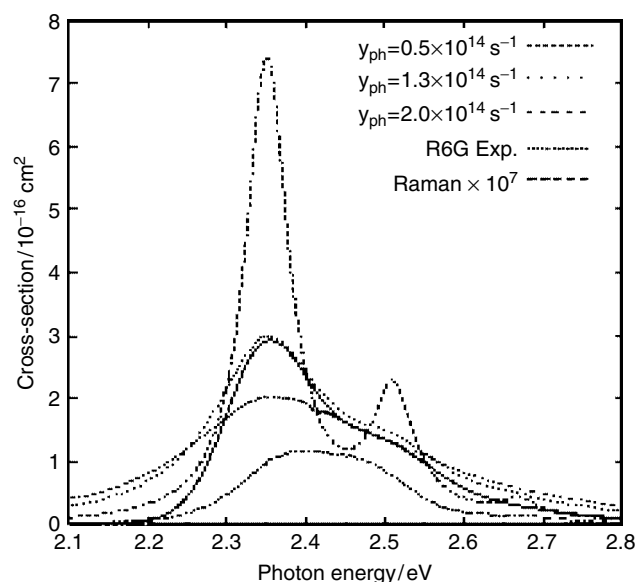


Figure 4. Calculated absorption spectrum and Raman excitation profile (total Raman cross-section as a function of incident laser photon energy) for the model molecule in free space. In addition, the experimental absorption spectrum for the R6G molecule is shown. Absorption spectra were calculated for a few different dephasing rates γ_{ph} ; as can be seen, the choice $\gamma_{ph} = 1.3 \times 10^{14} \text{ s}^{-1}$ gives the best agreement with experiment and was used when calculating the Raman profile. The other parameters entering the model are the dipole length $l_{dip} = 1.2 \text{ \AA}$, the Franck–Condon parameter $\alpha = 0.5$, $\hbar\Omega_{ge} = 2.35 \text{ eV}$ and $\hbar\Omega_{vib} = 160 \text{ meV} \approx 1300 \text{ cm}^{-1}$.

in Fig. 4. In order to achieve close agreement between the model spectrum and the experimental spectrum, a phenomenological dephasing rate γ_{ph} was included in the model.^{12,13} In simple terms, it accounts for the broadening of resonances in the real molecule, which has many more degrees of freedom than our model molecule. Figure 4 also illustrates the effects that a variation of γ_{ph} has on the absorption spectrum.

To calculate the molecule's fluorescence and Raman scattering cross-section σ per unit photon energy $\hbar\omega$ and unit solid angle Ω , we need to evaluate a dipole–dipole correlation function for the molecule's dipole moment $p(t)$:

$$\frac{d^2\sigma}{d\Omega d(\hbar\omega)} = \frac{\omega^4 |M(\omega)|^2}{I_{in} 8\pi^3 c^3 \epsilon_0 \hbar} \text{Re} \int_0^\infty e^{i\omega t} \langle p^{(-)}(0) p^{(+)}(t) \rangle dt \quad (2)$$

where the factor $|M(\omega)|^2$ is due to the enhanced radiation emission rate and I_{in} is the intensity of the incident laser light.

The dipole–dipole correlation function in general includes contributions to the emitted light due to both real transitions from the excited electronic level (fluorescence) and an oscillating dipole moment (Rayleigh and Raman scattering). To handle all these aspects in a general way, we

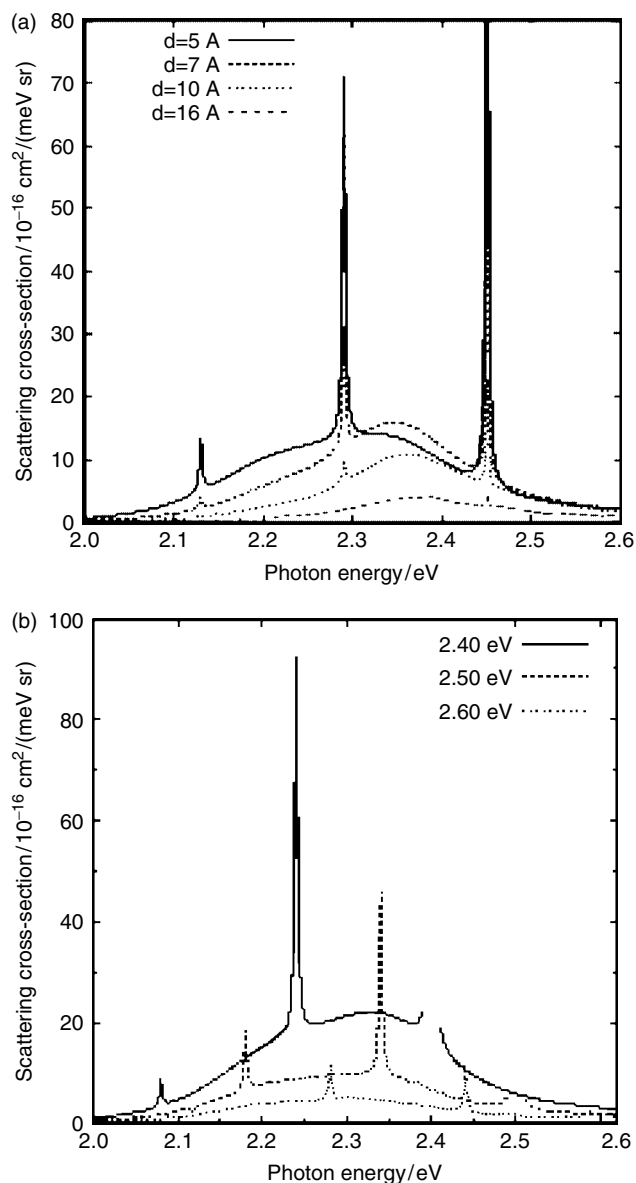


Figure 5. (a) Calculated Raman and fluorescence spectra for an R6G-like model molecule placed symmetrically between two Ag nanoparticles with radius 40 nm. The different curves were calculated with different molecule–particle separations as indicated. The laser photon energy $\hbar\omega_L = 2.45 \text{ eV}$, $\gamma_{\text{ph}} = 1.3 \times 10^{14} \text{ s}^{-1}$ and the other parameter values are the same as used in Fig. 4. The spectra show a broad fluorescence background with narrow peaks from Rayleigh scattering (at $\hbar\omega = \hbar\omega_L$) and Raman scattering (peaks red shifted with respect to $\hbar\omega_L$ by multiples of the vibrational quantum). (b) Spectra calculated in a similar way and with the same parameter values as in (a), but here the molecule–particle separation is always $d = 5 \text{ \AA}$, i.e. the gap distance is 1 nm, whereas the laser photon energy is varied as indicated.

use density-matrix methods to evaluate the scattering cross-section. Figure 5 gives some examples of how such spectra

can look. The spectra in Fig. 5(a) were calculated with a given set of parameter values (those used in Fig. 4) and fixed laser photon energy, 2.45 eV. The separation between the molecule and the nanoparticles, and thereby the field enhancement factors $M(\omega)$ and $M_d(\omega)$, are varied. For the smallest d , we obtain a large $M(\omega)$ and the Raman cross-section, which approximately scales as $|M(\omega)|^4$ as discussed above, produces prominent sharp peaks rising above the fluorescence background. With increasing d the enhancement diminishes and the Raman scattering decreases very rapidly. At $d = 16 \text{ \AA}$, it is very difficult to resolve the Raman peak. The fluorescence cross-section is also dependent on the electromagnetic enhancement and decreases with increasing d . However, this tendency is not as strong as for the Raman signal. The cross-section in this case scales approximately as $|M|^4/|M_d|^2$. Here a factor $|M(\omega)|^2$ is due to the enhanced emission rate, and the remaining factor $|M|^2/|M_d|^2$ indicates how the population of the excited electron state depends on the enhancement; the population is set by the ratio between the excitation rate from the ground state, proportional to $|M(\omega)|^2$, and the decay rate back, proportional to $|M_d(\omega)|^2$. For the smallest d studied here, $|M_d(\omega)|^2$ grows sufficiently fast due to dissipation processes in the particles that the fluorescence cross-section even begins to decrease. At the same time we note that this fluorescence ‘quenching’ is not as marked as in many experiments. This may indicate that processes not included in our model also are instrumental in reducing the fluorescence yield. However, calculations for a single sphere demonstrate a dramatic reduction in fluorescence yield, but in that case the Raman signal is far too low to allow for single molecule sensitivity (see Ref. 13).

Figure 5(b) shows how the combined Raman and fluorescence spectrum varies with incident laser frequency and illustrates the resonant nature of the Raman process, i.e. the fact that we are dealing with surface-enhanced resonance Raman scattering (SERRS).

CONCLUSIONS

The main advantage of the theoretical treatment outlined above is that it allows one to calculate absolute cross-sections and spectra. The energy integrated fluorescence cross-section of the free model molecule is $\sim 10^{-16} \text{ cm}^2$ according to the calculation, which is close to the experimental value for many fluorophores. The absorption cross-section is of a similar magnitude, i.e. the fluorescence quantum efficiency is close to unity. However, the integrated SERS cross-section is at least two orders of magnitude higher than the fluorescence cross-section of the free model molecule and thus ~ 15 orders of magnitude higher than a ‘typical’ Raman cross-section of a non-resonant molecule ($\sigma_R \approx 10^{-29} \text{ cm}^2$). However, this does not mean that the surface enhancement is 15 orders of magnitude. In order to obtain the true Raman enhancement factor, we have to compare with the resonant Raman cross-section of the free molecule. This value is very difficult

to obtain experimentally, because of the overwhelming fluorescence background, but it is accessible in the model calculation. Figure 4 shows that the relevant number is of the order $\sigma_R \approx 10^{-23} \text{ cm}^2$, which means that the true Raman enhancement factor is $\sim 10^{10}$. This value originates from the classical electrodynamic Raman enhancement $|M|^4$ at the 'hot spot' in the gap between the nanoparticles in Fig. 3. Hence no additional enhancement mechanisms beyond the 'electromagnetic SERS theory' are needed in order to explain quantitatively the enormous Raman signals observed in single-molecule SERRS experiments.

REFERENCES

1. Jeanmarie DL, Van Duyne RP. *J. Electroanal. Chem.* 1977; **84**: 1.
2. Moskovits M. *J. Chem. Phys.* 1978; **69**: 4159.
3. Ritchie RH. *Phys. Rev.* 1957; **106**: 874.
4. Barnes WL, Dereux A, Ebbesen TW. *Nature* 2003; **424**: 824.
5. Ebbesen TW, Lezec HJ, Ghaemi HF, Thio T, Wolff PA. *Nature* 1998; **391**: 667.
6. Andrew P, Barnes WL. *Science* 2004; **306**: 1002.
7. Homola J. *Anal. Bioanal. Chem.* 2003; **377**: 528.
8. O'Neal DP, Hirsch LR, Halas NJ, Payne JD, West JL. *Cancer Lett.* 2004; **209**: 171.
9. Maier SA, Kik PG, Atwater HA, Meltzer S, Harel E, Koel BE, Requicha AAG. *Nat. Mater.* 2003; **2**: 229.
10. Nie SM, Emory SR. *Science* 1997; **275**: 1102.
11. Kneipp K, Wang Y, Kneipp H, Perelman LT, Itzkan I, Dasari R, Feld MS. *Phys. Rev. Lett.* 1997; **78**: 1667.
12. Xu H-X, Wang X-H, Persson MP, Xu HQ, Käll M, Johansson P. *Phys. Rev. Lett.* 2004; **93**: 243 002.
13. Johansson P, Xu H-X, Käll M. *Physical Review B*, 71, in press.
14. Gersten J, Nitzan A. *J. Chem. Phys.* 1980; **73**: 3023.
15. Xu H-X. *Phys. Lett. A* 2003; **312**: 411.
16. Xu H-X. *J. Opt. Soc. Am. A* 2004; **21**: 804.
17. Xu H-X, Käll M. *ChemPhysChem* 2003; **4**: 1001.
18. Bosnick KA, Jiang J, Brus LE. *J. Phys. Chem. B* 2002; **106**: 8096.
19. Xu H-X, Aizpurua J, Käll M, Apell P. *Phys. Rev. E* 2000; **62**: 4318.